ESC European Society of Cardiology

Europace (2020) **22**, 1509–1519
doi:10.1093/europace/euaa130

CINICAL RESEARCH
Ablation for atrial fibrillation

Classification of sinus rhythm single potential morphology in patients with mitral valve disease

Mathijs S. van Schie[1], Roeliene Starreveld[1], Maarten C. Roos-Serote[1], Yannick J.H.J. Taverne[2], Frank R.N. van Schaagen[2], Ad J.J.C. Bogers[2] Natasja M.S. de Groot[1]*

[1]Department of Cardiology, Unit Translational Electrophysiology, Erasmus Medical Centre, Dr Molewaterplein 40, 3015GD Rotterdam, the Netherlands; and [2]Department of Cardiothoracic Surgery, Erasmus Medical Centre, Rotterdam, the Netherlands

Received 31 January 2020; revised 24 March 2020; editorial decision 25 April 2020; accepted after revision 28 April 2020; online publish-ahead-of-print 5 August 2020

Aims The morphology of unipolar single potentials (SPs) contains information on intra-atrial conduction disorders and possibly the substrate underlying atrial fibrillation (AF). This study examined the impact of AF episodes on features of SP morphology during sinus rhythm (SR) in patients with mitral valve disease.

Methods and results Intraoperative epicardial mapping (interelectrode distance 2 mm) of the right and left atrium (RA, LA), Bachmann's bundle (BB), and pulmonary vein area (PVA) was performed in 67 patients (27 male, 67 ± 11 years) with or without a history of paroxysmal AF (PAF). Unipolar SPs were classified according to their differences in relative R- and S-wave amplitude ratios. A clear predominance of S-waves was observed at BB and the RA in both the no AF and PAF groups (BB 88.8% vs. 85.9%, RA 92.1% vs. 85.1%, respectively). Potential voltages at the RA, BB, and PVA were significantly lower in the PAF group ($P < 0.001$ for each) and were mainly determined by the size of the S-waves amplitudes. The largest difference in S-wave amplitudes was found at BB; the S-wave amplitude was lower in the PAF group [4.08 (2.45–6.13) mV vs. 2.94 (1.40–4.75) mV; $P < 0.001$]. In addition, conduction velocity (CV) at BB was lower as well [0.97 (0.70–1.21) m/s vs. 0.89 (0.62–1.16) m/s, $P < 0.001$].

Conclusion Though excitation of the atria during SR is heterogeneously disrupted, a history of AF is characterized by decreased SP amplitudes at BB due to loss of S-wave amplitudes and decreased CV. This suggests that SP morphology could provide additional information on wavefront propagation.

Keywords Atrial fibrillation • Sinus rhythm • High-resolution epicardial mapping • Cardiac electrophysiology • Mitral valve disease • Mitral valve surgery

Introduction

Analysis of atrial electrical activity plays an important role in revealing the underlying electrophysiological mechanisms responsible for the initiation and perpetuation of atrial fibrillation (AF). In daily clinical practice, electroanatomical mapping is performed via endovascular catheters at the endocardial side, presenting a bipolar electrogram (EGM).[1,2] The bipolar EGM is commonly used as it contains local information from the area of myocardium at the catheter tip between two electrodes. However, unipolar EGMs have the benefit over bipolar EGMs that their morphology carries additional information about the progression of the wavefront and remote activations, which are

*Corresponding author. Tel: +31 10 7035018; fax: +31 10 7035258. *E-mail address*: n.m.s.degroot@erasmusmc.nl

What's new?

- This study examined the impact of atrial fibrillation (AF) episodes on features of unipolar single potential (SP) morphology at a high-resolution scale during sinus rhythm in 67 patients with mitral valve disease.
- A clear predominance of S-waves was observed at Bachmann's bundle (BB) and the right atrium in patients with and without history of paroxysmal AF.
- Paroxysmal AF is associated with decreased unipolar SP amplitudes at BB due to loss of S-wave amplitudes.
- Decreased unipolar SP amplitudes due to loss of S-wave amplitudes, together with a decreased conduction velocity, suggests that unipolar SP morphology could provide additional information on wavefront propagation.

independent of the electrode orientation and wavefront direction.[2] Cardiac electrophysiologists often rely on low-voltage areas which are suggestive of the presence of atrial substrate.[3] However, low-voltage potentials are highly determined by their morphology, but these are currently not fully classified in clinical practice. Therefore, unipolar EGMs can provide additional helpful information in electrophysiological studies and ablation procedures, and are therefore increasingly used in newly developed mapping systems.

The morphology of atrial EGMs, represented by the relative positive (R-wave) and negative (S-wave) components of a unipolar EGM, contains information on intra-atrial conduction and hence conduction disorders giving rise to development of AF.[2,4,5] Prior studies have indeed demonstrated that areas of abnormal EGM morphologies of single potentials (SPs) are indicators of conduction abnormalities underlying AF.[6–8] Therefore, creation of an electrical signal profile obtained from high-resolution mapping data of the entire atria during AF—a so-called AF Fingerprint—may be used to determine the severity and extensiveness of local conduction disorders. The first step towards development of such an 'AF Fingerprint', is understanding variation in EGM morphologies of SPs during sinus rhythm (SR). The goal of this study is therefore to examine the impact of AF episodes on features of SP morphology at a high-resolution scale during SR in patients with mitral valve disease (MVD).

Methods

Study population

The study population consisted of 67 adult patients undergoing mitral valve surgery or a combination of mitral valve and coronary bypass surgery in the Erasmus Medical Centre Rotterdam. This study was approved by the institutional medical ethical committee (MEC2010-054/MEC2014-393).[9,10] Written informed consent was obtained from all patients. Patient characteristics (e.g. age, medical history, cardiovascular risk factors, time in AF) were obtained from the patient's medical record. The study population was classified into patients without a history of AF (no AF group) and with a history of paroxysmal AF (PAF group).

Mapping procedure

Epicardial high-resolution mapping was performed prior to commencement of extra-corporal circulation, as previously described in detail.[11–13] A temporal bipolar epicardial pacemaker wire attached to the right atrial free wall served as a reference electrode. A steel wire fixed to subcutaneous tissue of the thoracic cavity was used as an indifferent electrode. Epicardial mapping was performed with a 128-electrode array or 192-electrode array (electrode diameter respectively 0.65 mm or 0.45 mm, interelectrode distances 2.0 mm). Mapping was conducted by shifting the electrode array along imaginary lines with a fixed anatomic orientation, following a predefined mapping scheme. The procedure covers the entire epicardial surface of the right atrium (RA), Bachmann's bundle (BB), pulmonary vein area (PVA), and left atrium (LA), as illustrated in the upper panel of left panel of *Figure 1*. Omission of areas was avoided at the expense of possible small overlap between adjacent mapping sites. The RA was mapped from the cavotricuspid isthmus, shifting perpendicular to the caval veins towards the right atrial appendage. The PVA was mapped from the sinus transversus fold along the borders of the right and left pulmonary veins (PVR and PVL) down towards the atrioventricular groove. The left atrioventricular groove was mapped from the lower border of the left inferior pulmonary vein towards the left atrial appendage. Bachmann's bundle was mapped from the tip of the left atrial appendage across the roof of the LA, behind the aorta towards the superior cavo-atrial junction.

Five seconds of SR were recorded from every mapping site, including a surface electrocardiogram lead, a calibration signal of 2 mV and 1000 ms, a bipolar reference EGM and all unipolar epicardial EGMs. In patients who presented in AF, SR mapping was performed after electrical cardioversion. Data were stored on a hard disk after amplification (gain 1000), filtering (bandwidth 0.5–400 Hz), sampling (1 kHz), and analogue to digital conversion (16 bits).

Data analysis

Unipolar EGM morphology was semiautomatically analysed in custom-made software using Python 3. EGMs with injury potentials, recording sites with ≥25% excluded or missing EGMs and premature atrial complexes or aberrant beats were excluded from analysis. Atrial deflections were marked when the negative slope of a deflection was ≥10% of the steepest slope in the EGM and the amplitude of the deflection was at least two times the signal-to-noise ratio of the EGM. The steepest negative deflection of a potential was marked as the local activation time. The minimal time between two successive deflections ('latency') was set to 2 ms. All EGM markings were manually checked and corrected in case of markings on electrical artefacts evaluated by a consensus of two investigators. Potentials were classified as SP (one deflection) or fractionated potential (FP, ≥2 deflections). Single potentials are characterized by a rapid negative deflection preceded by a positive R-wave and returning to the baseline (S-wave). As demonstrated in the lower panel of *Figure 1*, SPs were classified according to their differences in relative R- and S-wave amplitude and scaled from −1 (R-wave) to 1 (S-wave).

$$\mathrm{RS} = \begin{cases} 1 - \mathrm{RS}(n) & \text{for } \mathrm{RS}(n) \leq 1 \\ \dfrac{1}{\mathrm{RS}(n)} - 1 & \text{for } \mathrm{RS}(n) > 1 \end{cases}$$

Furthermore, SPs were analysed for peak-to-peak voltage (amplitude), relative R- and S-wave amplitudes and local wavefront conduction velocity (CV). Local CV was computed as an average of velocity estimations between neighbouring electrodes (longitudinal, transversal, and diagonal) based on a technique derived from a finite differences method developed and described by Salama *et al.*[14]

Statistical analysis

All data were tested for normality. Normally distributed data are expressed as mean ± standard deviation and analysed with a paired *T*-test

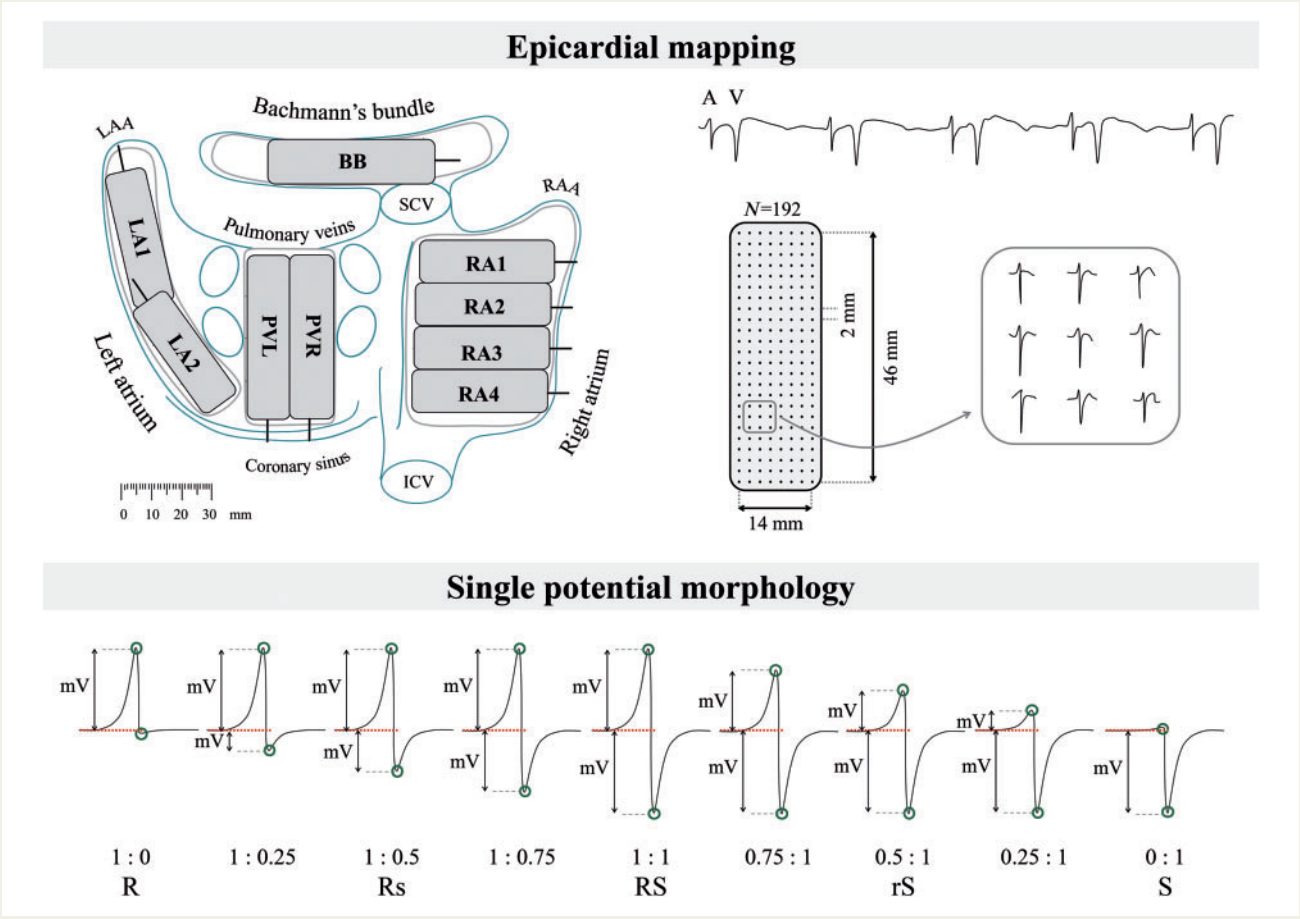

Figure 1 (*Upper left panel*) Projection of the 192-unipolar electrode array on a schematic posterior view of the atria. (*Upper right panel*) Epicardial, unipolar potentials recorded during 5 s of SR containing atrial deflections (A) and far-field ventricular signals (V). Typical examples of nine EGMs obtained from the RA are shown outside the mapping. (*Lower panel*) EGMs with variable R/S ratios calculated by dividing the R-wave amplitude by the S-wave amplitude. BB, Bachmann's bundle; EGM, electrogram; ICV, inferior caval vein; LA, left atrium; LAA, left atrial appendage; PV, pulmonary veins; RA, right atrium; RAA, right atrial appendage; SCV, superior caval vein; SR, sinus rhythm.

or one-way analysis of variance. Skewed data are expressed as median (25th–75th percentile) and analysed with a Kruskal–Wallis test or Mann–Whitney *U* test. Categorical data are expressed as numbers and percentages and analysed with a χ^2 or Fisher's exact test when appropriate. Distribution data were analysed with a two-sample Kolmogorov–Smirnov test. A *P*-value <0.05 was considered statistically significant. A Bonferroni correction was applied for comparison of the four atrial regions; a *P*-value of <0.0083 (0.05/6) was considered statistically significant.

Results

Study population

Clinical characteristics of the study population, including 44 patients in the 'no AF' group and 23 patients in the 'PAF' group are described in *Table 1*. These groups differed in age (no AF: 65 ± 13 years, PAF: 73 ± 6 years, $P = 0.003$). Patients had either ischaemic and MVD [no AF: 20 (45%), PAF: 6 (26%)] or only MVD. Left atrial dilation was present in 28 patients without AF (64%) and in 16 patients with PAF (70%). Most patients in both groups had normal left ventricular function [no AF: 29 (66%), PAF: 17 (74%)]. Thirty percent of the patients with PAF used class III antiarrhythmic drugs [no AF: 0 vs. PAF: 7 (30%), $P < 0.001$].

Mapping data

As demonstrated in *Table 2*, a total of 523 019 SPs were analysed out of 852 SR recordings of 5-s duration (no AF: RA: 179 700, BB: 34 069, PVA: 77 651, LA: 64 254; PAF: RA: 77 060; BB: 16 260; PVA: 38 720; LA: 35 305). Median unipolar SP amplitude in the PAF group was lower than in the no AF group [4.78 (2.14–7.21) mV vs. 5.05 (2.48–7.64) mV, respectively ($P < 0.001$)].

In both the no AF and PAF group, SP amplitudes differed between the atrial regions [no AF: RA: 5.21 (3.03–7.67) mV, BB: 5.71 (3.40–8.87) mV, PVA: 4.48 (2.03–8.19) mV, LA: 4.72 (2.19–8.24) mV ($P < 0.001$ for all comparisons); PAF group: RA: 5.10 (2.89–7.55) mV, BB: 4.09 (2.18–6.70) mV, PVA: 4.36 (1.95–8.38) mV, LA: 4.74 (2.47–7.63) mV ($P < 0.001$ for all comparisons)]. Furthermore, SP amplitudes of the RA, BB and PVA were lower in the PAF group compared to the no AF group [RA: 5.21 (3.03–7.67) mV vs. 5.10 (2.89–7.55) mV ($P < 0.001$), BB: 5.71 (3.40–8.87) mV vs. 4.09 (2.18–6.70) mV

Table 1 Patient characteristics (*N* = 67)

	No AF	PAF	*P*-value
Patients	44 (66)	23 (34)	–
Male	17 (39)	10 (43)	0.903
Age (years)	65 ± 12	73 ± 6	0.003
Cardiovascular risk factors			
BMI (kg/m^2)	24.5 (22.1–26.8)	25.3 (22.2–31.9)	0.281
Underweight (<18.5)	2 (5)	0 (0)	0.778
Normal weight (18.5–25)	22 (50)	11 (48)	0.866
Overweight (25–30)	15 (34)	5 (22)	0.443
Obese (≥30)	5 (11)	7 (30)	0.110
Hypertension	15 (34)	12 (52)	0.242
Dyslipidaemia	14 (32)	2 (9)	0.071
Diabetes mellitus	7 (16)	3 (13)	0.755
Left atrial dilatation >45 mm	28 (64)	16 (70)	0.830
Left ventricular dysfunction	15 (34)	6 (26)	0.694
Mitral stenosis	3 (7)	1 (4)	0.685
Severe mitral insufficiency	31 (70)	16 (70)	0.940
Coronary artery disease	20 (45)	6 (26)	0.200
Antiarrhythmic agents			
Class I	1 (2)	0 (0)	0.466
Class II	23 (52)	11 (48)	0.930
Class III	0 (0)	7 (30)	<0.001
Class IV	1 (2)	2 (9)	0.559

Values are presented as mean ± standard deviation, median (interquartile ranges), or as *n* (%).
BMI, body mass index; (P)AF, (paroxysmal) atrial fibrillation.

(*P* < 0.001), PVA: 4.48 (2.03–8.19) mV vs. 4.36 (1.95–8.38) mV (*P* < 0.001)].

Focusing only on the magnitude of the R- and S-wave, the largest R-wave amplitude was found in the LA in both the no AF group [2.44 (1.13–4.39) mV] and PAF group [2.24 (1.21–3.94) mV], whereas the largest S-wave amplitude was found in BB in the no AF group [4.08 (2.45–6.13) mV] and in the RA in the PAF group [3.30 (1.86–4.97) mV]. In general, the amplitude of the atrial potential was mainly determined by the S-wave amplitude.

The largest difference in S-wave amplitudes between both groups was found at BB; the S-wave median amplitude was higher in the no AF group [4.08 (2.45–6.13) mV] than in the PAF group [2.94 (1.40–4.75) mV; *P* < 0.001].

The CV differed between atrial regions in both the no AF and PAF group [no AF: RA: 0.93 (0.71–1.15) m/s, BB: 0.97 (0.70–1.21) m/s, PVA: 0.98 (0.66–1.25) m/s, LA: 0.91 (0.54–1.23) m/s (*P* < 0.001 for all comparisons); PAF group: RA: 0.94 (0.72–1.17) m/s, BB: 0.89 (0.62–1.16) m/s, PVA: 1.00 (0.70–1.25) m/s, LA: 0.94 (0.60–1.24) m/s (*P* < 0.001 for all comparisons)]. In the PAF group, CVs at BB were lower compared to the no AF group [0.97 (0.70–1.21) m/s vs. 0.89 (0.62–1.16) m/s, *P* < 0.001].

Regional differences in R/S ratio

Figure 2 shows a typical example of the colour-coded spatial distribution of the R/S ratios during one SR beat in a patient without AF. This map shows a wide variation of R/S ratios throughout the atria. The majority of the SPs recorded in the superior part of RA consisted of monophasic S-waves, compared to rS-waves and biphasic RS-waves in the mid and inferior part of the RA. A clear R-wave predominance was found in between the pulmonary veins, whereas biphasic RS-waves and rS-waves were recorded from the superior and inferior sites of the PVA. The LA appendage revealed a R-wave predominance as well, whereas S-wave predominance was mainly found in the RA and BB.

Figure 3 shows the regional differences in the distribution of the R/S ratios in the RA, BB, PVA and LA in the no AF group (upper panels) and PAF group (lower panels). The relative frequency of the R/S ratios are ranked from −1 (R-waves) to 1 (S-waves) and divided into four equal quartiles. For each quartile, the relative number of potentials is given on top of the plots. The SPs revealed a wide variation of R- and S-wave amplitude ratios. However, a clear predominance of S-waves was observed in the BB and RA in both the no AF group (88.8% and 92.1%, respectively) as PAF group (85.9% and 85.1%, respectively). Differences between the no AF and PAF groups were found at the RA, BB and LA (*P* = 0.021, *P* = 0.003, and *P* = 0.013). In the PAF group, there was a larger number of dominant R-waves in both the RA and BB and a higher number of rS-waves in the LA.

Individual differences in R/S ratios

Figure 4 demonstrates interindividual differences in R/S ratios. In all patients, there was a clear S-wave predominance in the RA and BB. In contrast, in the PVA and LA, there was less S-wave predominance and a wider variation in SP morphology.

Table 2 Mapping data characteristics (*N* = 523 019)

	No AF	PAF	*P*-value
Right atrium			
Single potentials	179 700 (85)	77 060 (85)	
Amplitude (mV)	5.21 (3.03–7.67)	5.10 (2.89–7.55)	<0.001
R-wave (mV)	1.65 (0.74–2.79)	1.69 (0.79–2.81)	<0.001
S-wave (mV)	3.48 (2.07–5.08)	3.30 (1.86–4.97)	<0.001
R/S ratio	0.52 (0.28–0.71)	0.46 (0.22–0.67)	<0.001
Conduction velocity (m/s)	0.93 (0.71–1.15)	0.94 (0.72–1.17)	<0.001
Bachmann's bundle			
Single potentials	34 069 (76)	16 260 (73)	
Amplitude (mV)	5.71 (3.40–8.87)	4.09 (2.18–6.70)	<0.001
R-wave (mV)	1.57 (0.74–3.00)	1.11 (0.49–2.21)	<0.001
S-wave (mV)	4.08 (2.45–6.13)	2.94 (1.40–4.75)	<0.001
R/S ratio	0.57 (0.35–0.76)	0.58 (0.29–0.77)	<0.001
Conduction velocity (m/s)	0.97 (0.70–1.21)	0.89 (0.62–1.16)	<0.001
Left atrium			
Single potentials	64 254 (84)	35 305 (83)	
Amplitude (mV)	4.72 (2.19–8.24)	4.74 (2.47–7.63)	0.067
R-wave (mV)	2.44 (1.13–4.39)	2.24 (1.21–3.94)	<0.001
S-wave (mV)	1.91 (0.83–3.89)	2.12 (0.93–3.86)	<0.001
R/S ratio	−0.16 (−0.52 to 0.30)	−0.03 (−0.46 to 0.38)	<0.001
Conduction velocity (m/s)	0.91 (0.54–1.23)	0.94 (0.60–1.23)	<0.001
Pulmonary vein area			
Single potentials	77 651 (87)	38 720 (77)	
Amplitude (mV)	4.48 (2.03–8.19)	4.36 (1.95–8.38)	<0.001
R-wave (mV)	1.94 (0.94–3.72)	1.98 (0.84–4.10)	0.177
S-wave (mV)	2.28 (0.92–4.12)	2.13 (0.94–4.22)	<0.001
R/S ratio	0.14 (−0.33–0.45)	0.12 (−0.29–0.44)	0.156
Conduction velocity (m/s)	0.98 (0.66–1.25)	1.00 (0.70–1.25)	<0.001

Values are presented as median (interquartile range) or as *n* (%).
(P)AF, (paroxysmal) atrial fibrillation.

Figure 5 demonstrates all R/S ratios (subdivided into nine categories) with their corresponding amplitudes. In both the no AF and PAF group, the largest SP amplitudes were observed in the range of biphasic RS- to rS-waves [no AF: RA: 6.39 (4.25–8.89) mV, BB: 7.61 (4.51–12.55) mV, PVA: 5.96 (3.30–9.86) mV, LA: 6.77 (3.78–10.95) mV; PAF: RA: 5.96 (3.83–8.34) mV, BB: 5.45 (2.78–9.28) mV, PVA: 6.10 (3.21–10.44) mV, LA: 6.02 (3.53–8.90) mV]. In the PAF group, SP amplitudes of all different R/S ratios were smaller in BB compared to the no AF group ($P < 0.001$). At the other atrial regions, there were no consistent significant differences in amplitudes of the various R/S ratios. The majority of the monophasic S-wave potentials were found in the RA in both groups (4.2% and 4.3%, respectively). A high number of S-wave potentials (3.7% for both groups) were found in BB as well, whereas these potentials were rarely present in the PVA and LA.

R/S ratio in low-voltage areas

The p5 of all measured SPs was 1.0 mV, which was used as a cut-off value for low voltages. *Figure 6* illustrates the regional distribution of the R/S ratios of low-voltage potentials. Although a wide variation of R/S ratios was observed, an S-wave predominance was found in the RA and BB in both groups. Compared to the no AF group, the relative number of dominant R-waves in low-voltage areas in the PAF group was larger in the RA and BB, whereas a larger number of dominant S-waves was observed in the PVA.

Discussion

High-resolution mapping of the atria in patients with MVD demonstrated a wide variation of unipolar SP morphology throughout the atria, resulting in specific regional differences in SP amplitude and R/S ratios. Amplitudes were mainly determined by the S-wave amplitude, which resulted in a high number of predominant S-wave potentials with large amplitudes in the RA and BB, whereas a larger range of SP amplitudes was found in the LA and PVA together with a high variation in R/S ratios. Compared to the no AF group, lower SP amplitudes and S-wave amplitudes were found in patients with PAF, along with more R-wave predominance in the RA, BB, and PVA.

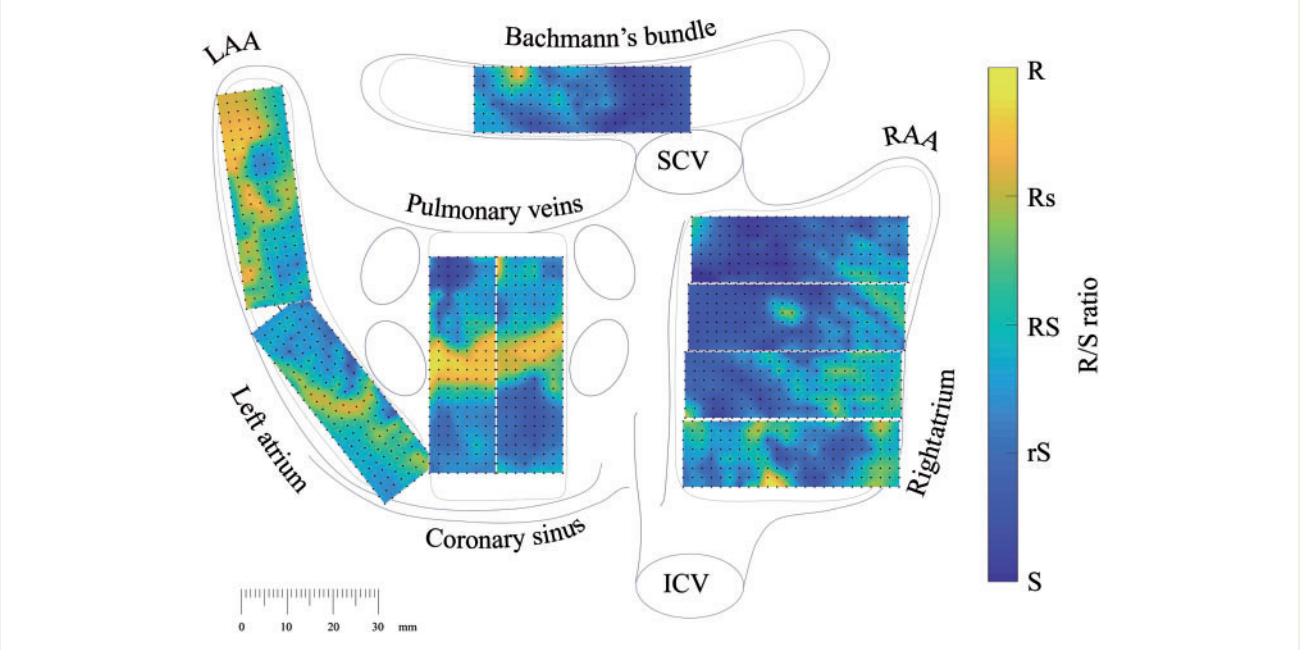

Figure 2 Typical example of the colour-coded spatial distribution of the R/S ratios during one sinus beat in a patient without AF. The colour scale of the R/S ratios ranges from S-waves (blue), via biphasic RS-waves (green) to R-waves (yellow). AF, atrial fibrillation; LAA, left atrial appendage; ICV, inferior caval vein; RAA, right atrial appendage; SCV, superior caval vein.

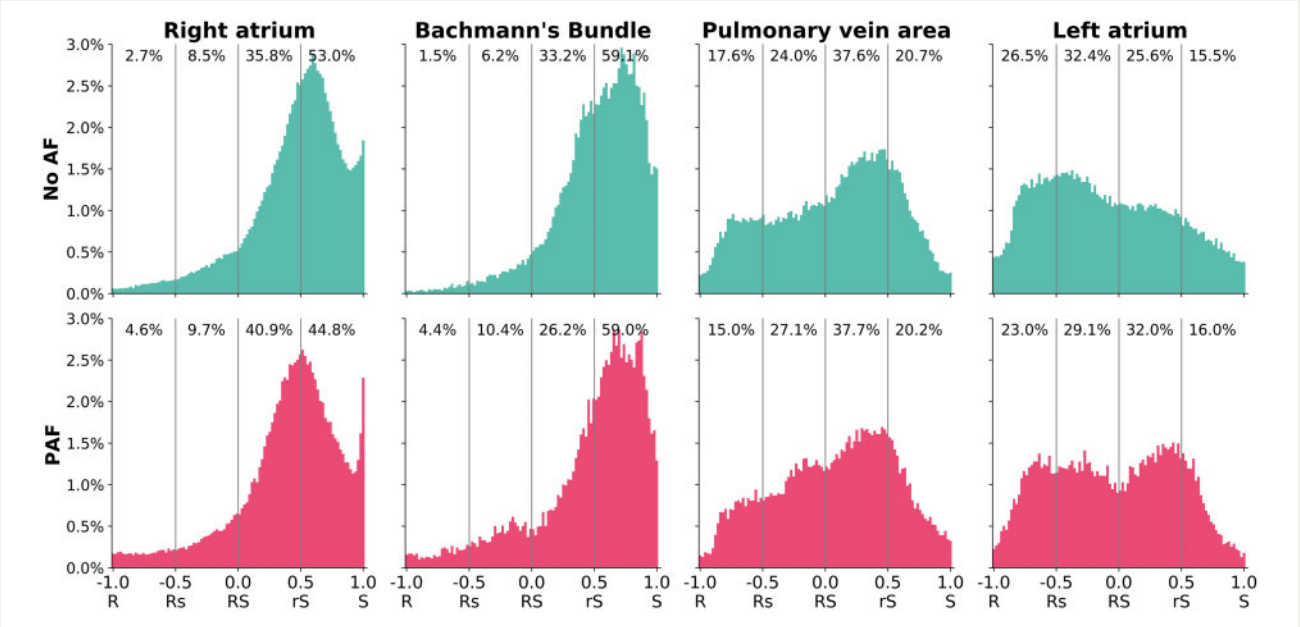

Figure 3 Relative frequency histograms of the R/S ratios of unipolar SPs during SR in patients without AF (turquoise) and patients with PAF (red), recorded from BB (n = 34,069 vs. n = 16 260), LA (n = 64 254 vs. n = 35 305), PVA (n = 77 651 vs. n = 38 720), and RA (n = 179 700 vs. n = 77 060). The histograms are divided into four equal quartiles; for each quartile, the relative number of potentials is given on top of the plots. BB, Bachmann's bundle; LA, left atrium; (P)AF, (paroxysmal) atrial fibrillation; PVA, pulmonary vein area; RA, right atrium; SP, single potential; SR, sinus rhythm.

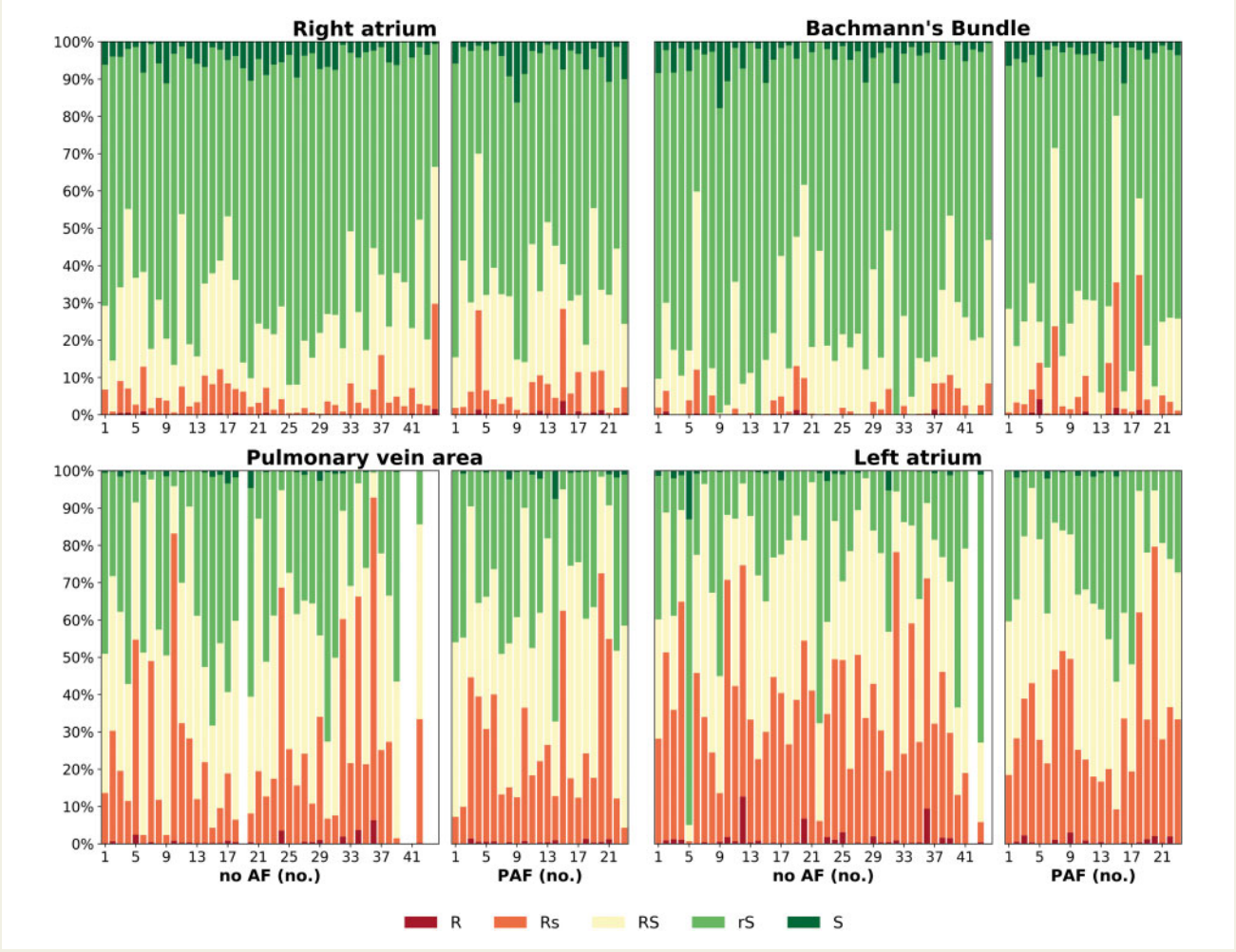

Figure 4 Stacked bar plots of the R/S distributions depicted for each patient separately in the RA, BB, PVA, and LA. BB, Bachmann's bundle; LA, left atrium; (P)AF, (paroxysmal) atrial fibrillation; PVA, pulmonary vein area.

Genesis of unipolar potential morphologies

Electrogram morphology is often used for the identification of structural or electrical remodelled areas with arrhythmogenic properties. In most settings, electro-anatomical mapping is performed via endovascular catheters at the endocardial side, recording EGMs which are the product of a voltage difference between recording electrodes (bipolar recordings).[1,15] In case of unipolar EGMs, the signal reflects the cardiac electrical activity of the tissue surrounding the recording electrode which decreases with distance. It is obtained by an exploring electrode positioned in the heart and an indifferent electrode located at an infinite distance.[2,16] It is for these reasons that there is an increase in mapping systems using unipolar EGMs.

The morphology of unipolar potentials can be regarded as the sum of instantaneous current dipoles of a wavefront, generating a positive deflection when the activation wavefront propagates towards the electrode and a steeply negative deflection as the wavefront reaches the electrode and propagates away, thereby generating a biphasic RS-wave.[2,5,17] When the electrode is located at a site of initial activation, depolarization produces a wavefront that propagates radially away from the electrode, thus generating a monophasic S-wave. In contrast, positive R-waves are characteristic of termination of the activation wavefront. Areas of fast conduction with conduction along the longitudinal axis of the fibres are characterized by large amplitude RS-waves, whereas in slow areas the potentials are of lower amplitude.[5] Abnormal myocardial substrate can be defined by substrate mapping by identifying areas of low voltage, as amplitude also depends on the volume of simultaneously activated cardiac tissue.[5,6] In addition, asymmetry of unipolar potentials has been proposed as a morphology parameter, determined by wavefront curvature, wavefront collisions, anisotropy, and conduction heterogeneity.[18,19]

Regional differences in single potential morphology

In our study population, there were clear regional differences in potential morphology. During SR, the initial excitation site is located in

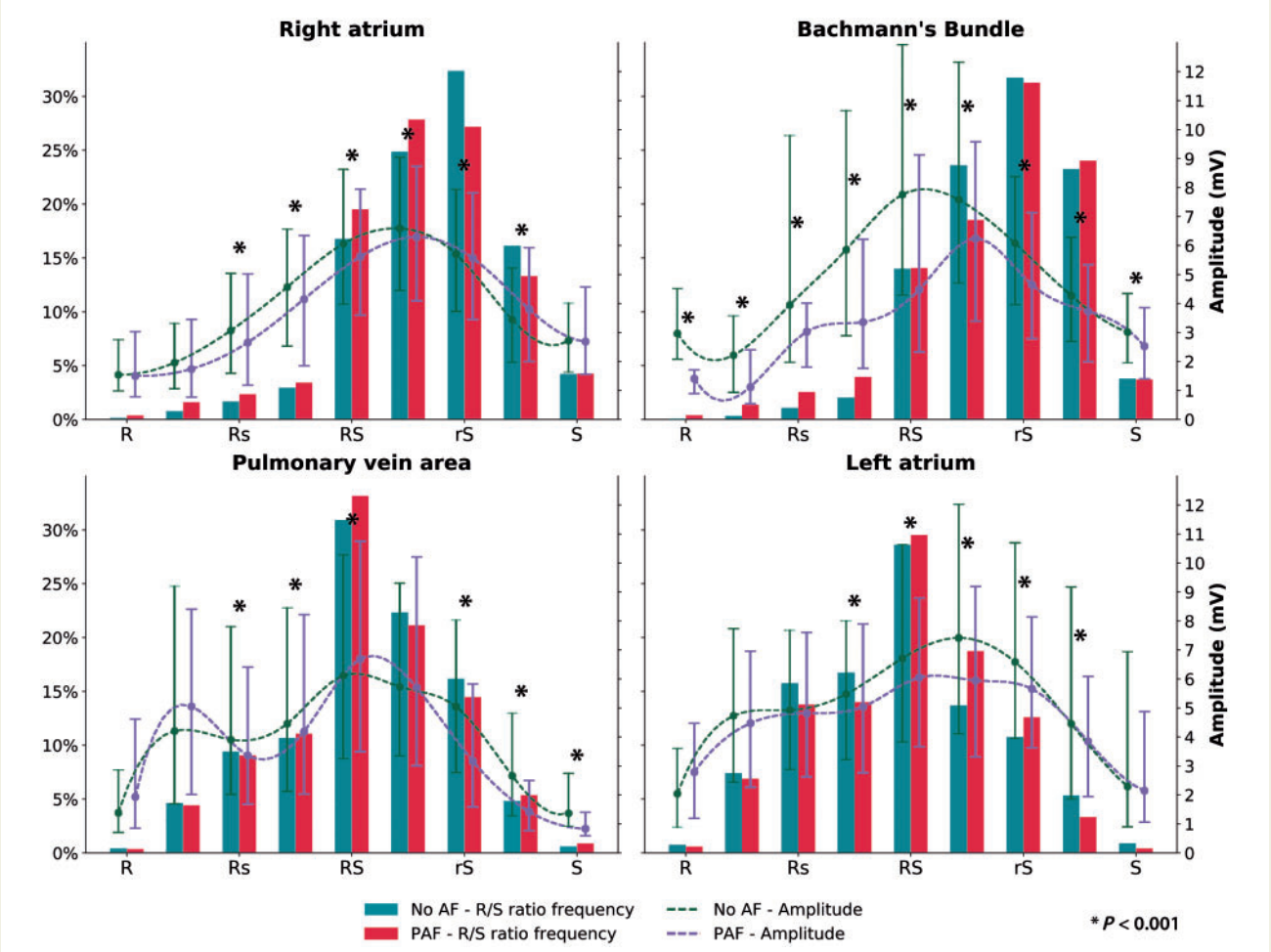

Figure 5 Relative frequency histograms of the R/S ratios and amplitudes of unipolar SPs during SR in patients without AF (turquoise) and with PAF (red). The bars represent the relative frequency of the R/S ratios and the dotted line the median amplitudes with interquartile ranges. The asterisk indicates a significant difference in median amplitudes between the patients without AF and patients with PAF ($P < 0.001$). (P)AF, (paroxysmal) atrial fibrillation.

the RA in which wavefronts are generated by cells in the sinoatrial (SA) node area. From there, a wavefront is propagated by the prominent muscle bundles contiguous with the SA node; i.e. the crista terminalis, BB and the septo-pulmonary bundle, which contributes to fast electrical propagation and enables efficient electromechanical coupling of both atria during each normal sinus beat.[4,20] At sites of wavefront activation, monophasic S-waves were expected and were—indeed—mainly recorded in the RA in our study population. In addition, fast propagating wavefronts are characterized by EGMs with large amplitude, predominant S-waves, which evolve towards biphasic RS-waves when the wavefront propagates away from the excitation site. These types of potentials were indeed mainly found in the RA and BB.

Using diffusion tensor imaging of human hearts, Pashakhanloo *et al.*[21] have demonstrated that in some areas of the atrial wall, e.g. the crista terminalis and the antrum of the PVs, the uniform distribution of myocardial fibres is disrupted by multiple complex crossings of multiple fibres, which underlies non-uniform anisotropic propagation. Previous studies have demonstrated that there are changes in patients with MVD in the myocardial structure of the atria due to altered hemodynamic effects.[22–24] Structural remodelling affects intra-atrial conduction and thereby predisposes to development of atrial tachyarrhythmias. The higher incidence of AF in patients with MVD suggests the presence of a higher degree of atrial remodelling in these patients, characterized by LA enlargement, loss of myocardium and scarring.[25–27] The resulting anisotropic propagation causes local wavefront termination or collision, resulting in more R-wave predominance and monophasic R-waves, which were—indeed—mainly found in the LA and PVA.

In our study, we demonstrated inter-individual differences in R/S ratios in—especially—the LA and PVA areas. Anatomic studies of the fibre orientation using dissection, visual tracing or MR techniques demonstrated variations in the location and orientation of bundles between human hearts, in which mixed and oblique patterns of fibres were present in the roof of the atria encircling the pulmonary veins.[21,28] In addition, intraoperative epicardial mapping also demonstrated that atrial excitation during SR is affected by the underlying heart disease and AF, resulting in alternative routes for BB and PVA with high inter-individual variability.[29,30] Together

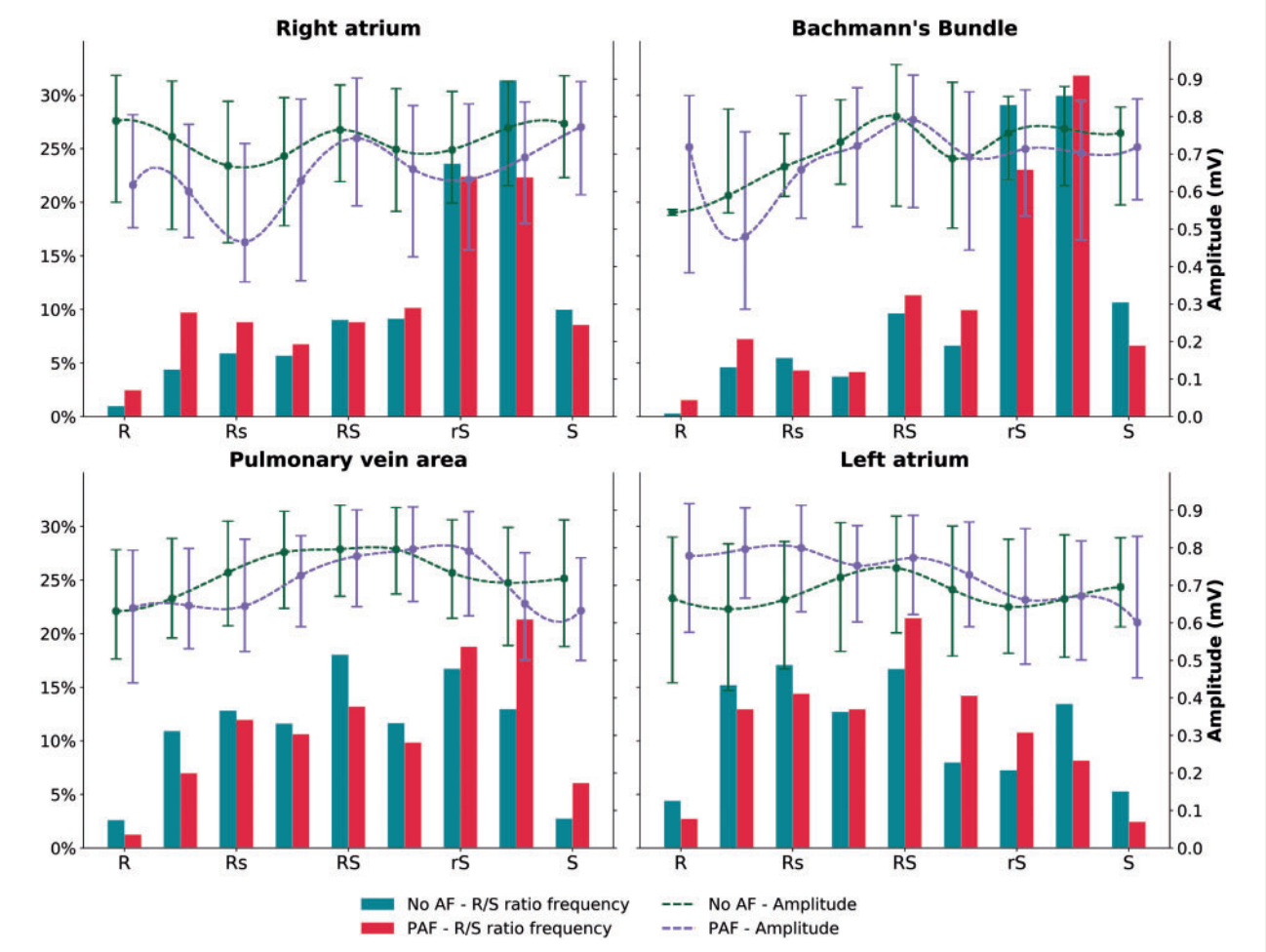

Figure 6 Relative frequency histograms of the RS ratios and amplitudes of unipolar SPs in low-voltage areas during SR in patients without AF (turquoise) and with PAF (red). The bars represent the relative frequency of the R/S ratios and the dotted line the median amplitudes with interquartile ranges. (P)AF, (paroxysmal) atrial fibrillation; SP, single potential; SR, sinus rhythm.

with the patient-specific impact of the presence of MVD, these differences might have resulted in the more prominent inter-individual R/S differences in these areas.

Several computer models of electrical propagation in the atria have been developed and showed mostly single biphasic potentials in the uniform atria, whereas dominant S-waves were more common in anisotropic tissue and dominant R-waves were found due to the multiple collisions.[19] Using such computer models it has been demonstrated that anisotropy has a greater impact on amplitude variation and asymmetry than the shape and curvature of the conducting wavefront. However, the models differ in the level of electrophysiological and anatomical details, such as fibre orientation, presence of the main muscle bundles, structural modifications and anisotropy, and mainly focus on arrhythmia simulations.[19,31–34] S-wave predominance has also been reported in the RA in patients during AF but could not be strongly correlated to wavefront curvature or anisotropy.[35] A tilted transmural stance of the wavefront resulting in an epicardial lead with constant epicardial to endocardial activation was proposed as a theoretical explanation for S-wave predominance during AF, which would present with more R-wave predominance at the endocardium.[35] However, Van der Does *et al.*[36] reported that both epicardial and endocardial EGMs showed an S-wave predominance, and endocardial EGMs did not have higher R/S ratios than epicardial EGMs Though these mapping studies were performed during SR, data clearly showed absence of an oblique transmurally propagating wave. In our study, we indeed demonstrated an S-wave predominance in the RA but not in the LA and PVA.

Influence of paroxysmal atrial fibrillation

In our study, SP morphology differences between patients without AF and with PAF were most prominent in the BB. Patients with PAF had lower amplitudes, more R-wave predominance, and slower wavefront propagation. The lower amplitude was mainly determined by a decrease in S-wave amplitude, which is observed with reversible tissue injury and is associated with conduction block during ablative therapy.[18,37] Recent studies indeed found more conduction abnormalities at BB during SR in patients with AF or patients who

developed post-operative AF.[11,38] BB is by far the largest of the anatomic interatrial connections and probably accounts for the largest part of interatrial conduction. It is a highly organized bundle of muscular fibres arranged in parallel fashion, but due to its anisotropic features BB is more vulnerable to structural remodelling that can even be identified during SR. In addition, the muscular fibres of BB are not enclosed by fibrous tissue and may therefore also be vulnerable to disruption by stretch due to the hemodynamic changes in the atria caused by MVD.[20,22,39] This could lead to slower wavefront propagation and slower CVs which were—indeed—found in patients with PAF. Structural changes of the atrial myocardium are more extensive in patients with PAF than in patients without AF, especially involving the BB.[40]

Clinical implications

Despite most of atrial mapping procedures are performed endocardially using bipolar EGMs, there is an increase in mapping systems using unipolar EGMs. Therefore, detailed knowledge of unipolar EGM morphology becomes more important. In a prior study of Van der Does *et al.*,[36] no differences were found between unipolar endo- and epicardial EGMs This indicates that the observed change in R/S ratios and decrease of S-wave amplitudes will also be found at the endocardium.

In clinical practice, low-voltage areas are regarded as part of the arrhythmogenic substrate underlying AF. However, our data shows that the EGM voltage is mainly determined by the R/S ratio which differs per region. In addition, low peak-to-peak voltages do not automatically indicate 'diseased' tissue, but can also be explained by the potential morphology as R- and S-waves have a smaller amplitude compared to RS-waves. Therefore, using voltage mapping alone to guide ablative therapy might be misleading.

Limitations

Whether general anaesthesia and intraoperative drugs influence conduction is unknown; however, a standard anaesthetic protocol was used for all patients and SR was confirmed during all mapping procedures. Therefore, possible effects of anaesthesia would be equally dispersed among the patient population. High-resolution mapping of the interatrial septum could not be performed with our closed beating heart approach.

Several patients with history of AF used antiarrhythmic drugs class III. Amiodarone has Class I antiarrhythmic properties via inhibition of sodium channels during phase 0 of the cardiac action potential which can slow intra-atrial conduction. Therefore, the use of amiodarone could have affected our results.

There was a difference in age between the no AF and PAF group. Therefore, the differences between both groups could be related to the impact of age. However, no correlation was found between any of signal profiles and age. Still, the possible effect could not be completely excluded, just as the effects of hypertension or obesity, although not significantly different between the groups.

Conclusion

A specific regional distribution of EGM morphology, involving R/S ratios, EGM voltage, and R- and S-wave amplitudes exist during SR in patients with MVD. Though excitation of the atria during SR is heterogeneously disrupted in patients with MVD, the occurrence of AF in this patient group is characterized by decreased SP amplitudes at BB due to loss of S-wave amplitudes together with a decreased CV. Therefore, BB is an area that could especially be interesting for AF Fingerprinting. Our findings that variation in EGM morphologies in our population is considerable—particularly at the LA and PVA—and specific EGM morphologies at regions such as BB are related to AF suggests that the potential morphology could provide additional information on CV and wavefront propagation, and emphasizes the need for a diagnostic tool enabling identification of arrythmogenic substrate in the individual patient.

Acknowledgements

The authors would like to kindly thank J.A. Bekkers, MD, PhD; W.J. van Leeuwen, MD; F.B.S. Oei, MD, PhD; P.C. van de Woestijne, MD; A. Yaksh, MD, PhD; C.P. Teuwen, MD; E.A.H. Lanters, MD; J.M.E. van der Does, MD; C.S. Serban, DVM; R.K. Kharbanda, MD; L.N. van Staveren, MD; A. Heida, MD; W.F.B. van der Does, MD; for their contribution to this work.

Funding

This work was supported by funding grants from CVON-AFFIP [914728]; NWO-Vidi [91717339]; Biosense Webster USA [783454]; and Medical Delta to N.M.S.d.G.

Conflict of interest: none declared.

Data availability

The data underlying this article will be shared on reasonable request to the corresponding author.

References

1. Koutalas E, Rolf S, Dinov B, Richter S, Arya A, Bollmann A *et al.* Contemporary mapping techniques of complex cardiac arrhythmias—identifying and modifying the arrhythmogenic substrate. *Arrhythm Electrophysiol Rev* 2015;**4**:19–27.
2. Stevenson WG, Soejima K. Recording techniques for clinical electrophysiology. *J Cardiovasc Electrophysiol* 2005;**16**:1017–22.
3. Wong GR, Nalliah CJ, Lee G, Voskoboinik A, Prabhu S, Parameswaran R *et al.* Dynamic atrial substrate during high-density mapping of paroxysmal and persistent AF: implications for substrate ablation. *JACC Clin Electrophysiol* 2019;**5**:1265–77.
4. Spach MS, King TD, Barr RC, Boaz DE, Morrow MN, Herman-Giddens S. Electrical potential distribution surrounding the atria during depolarization and repolarization in the dog. *Circ Res* 1969;**24**:857–73.
5. Spach MS, Miller WT 3rd, Miller-Jones E, Warren RB, Barr RC. Extracellular potentials related to intracellular action potentials during impulse conduction in anisotropic canine cardiac muscle. *Circ Res* 1979;**45**:188–204.
6. de Groot NM, Schalij MJ, Zeppenfeld K, Blom NA, Van der Velde ET, Van der Wall EE. Voltage and activation mapping: how the recording technique affects the outcome of catheter ablation procedures in patients with congenital heart disease. *Circulation* 2003;**108**:2099–106.
7. Otomo K, Uno K, Fujiwara H, Isobe M, Iesaka Y. Local unipolar and bipolar electrogram criteria for evaluating the transmurality of atrial ablation lesions at different catheter orientations relative to the endocardial surface. *Heart Rhythm* 2010;**7**:1291–300.
8. Bortone A, Appetiti A, Bouzeman A, Maupas E, Ciobotaru V, Boulenc JM *et al.* Unipolar signal modification as a guide for lesion creation during radiofrequency application in the left atrium: prospective study in humans in the setting of paroxysmal atrial fibrillation catheter ablation. *Circ Arrhythm Electrophysiol* 2013;**6**:1095–102.
9. Lanters EA, van Marion DM, Kik C, Steen H, Bogers AJ, Allessie MA *et al.* HALT & REVERSE: Hsf1 activators lower cardiomyocyt damage; towards a novel approach to REVERSE atrial fibrillation. *J Transl Med* 2015;**13**:347.

10. van der Does LJ, Yaksh A, Kik C, Knops P, Lanters EA, Teuwen CP *et al*. QUest for the Arrhythmogenic Substrate of Atrial fibRillation in Patients Undergoing Cardiac Surgery (QUASAR study): rationale and design. *J Cardiovasc Transl Res* 2016;**9**:194–201.
11. Teuwen CP, Yaksh A, Lanters EA, Kik C, van der Does LJ, Knops P *et al*. Relevance of conduction disorders in Bachmann's bundle during sinus rhythm in humans. *Circ Arrhythm Electrophysiol* 2016;**9**:e003972.
12. Mouws E, Lanters EAH, Teuwen CP, van der Does L, Kik C, Knops P *et al*. Epicardial breakthrough waves during sinus rhythm: depiction of the arrhythmogenic substrate? *Circ Arrhythm Electrophysiol* 2017;**10**:e005145.
13. Kik C, Mouws E, Bogers A, de Groot N. Intra-operative mapping of the atria: the first step towards individualization of atrial fibrillation therapy? *Expert Rev Cardiovasc Ther* 2017;**15**:537–45.
14. Salama G, Kanai A, Efimov IR. Subthreshold stimulation of Purkinje fibers interrupts ventricular tachycardia in intact hearts. Experimental study with voltage-sensitive dyes and imaging techniques. *Circ Res* 1994;**74**:604–19.
15. Friedman PA. Novel mapping techniques for cardiac electrophysiology. *Heart* 2002;**87**:575–82.
16. Blanchard SM, Damiano RJ Jr, Asano T, Smith WM, Ideker RE, Lowe JE. The effects of distant cardiac electrical events on local activation in unipolar epicardial electrograms. *IEEE Trans Biomed Eng* 1987;**34**:539–46.
17. Cantwell CD, Roney CH, Ng FS, Siggers JH, Sherwin SJ, Peters NS. Techniques for automated local activation time annotation and conduction velocity estimation in cardiac mapping. *Comput Biol Med* 2015;**65**:229–42.
18. Villacastin J, Almendral J, Arenal A, Castellano NP, Gonzalez S, Ortiz M *et al*. Usefulness of unipolar electrograms to detect isthmus block after radiofrequency ablation of typical atrial flutter. *Circulation* 2000;**102**:3080–5.
19. Jacquemet V, Virag N, Ihara Z, Dang L, Blanc O, Zozor S *et al*. Study of unipolar electrogram morphology in a computer model of atrial fibrillation. *J Cardiovasc Electrophysiol* 2003;**14**:S172–179.
20. Ho SY, Anderson RH, Sanchez-Quintana D. Atrial structure and fibres: morphologic bases of atrial conduction. *Cardiovasc Res* 2002;**54**:325–36.
21. Pashakhanloo F, Herzka DA, Ashikaga H, Mori S, Gai N, Bluemke DA *et al*. Myofiber architecture of the human atria as revealed by submillimeter diffusion tensor imaging. *Circ Arrhythm Electrophysiol* 2016;**9**:e004133.
22. Anne W, Willems R, Roskams T, Sergeant P, Herijgers P, Holemans P *et al*. Matrix metalloproteinases and atrial remodeling in patients with mitral valve disease and atrial fibrillation. *Cardiovasc Res* 2005;**67**:655–66.
23. Castonguay MC, Wang Y, Gerhart JL, Miller DV, Stulak JM, Edwards WD *et al*. Surgical pathology of atrial appendages removed during the cox-maze procedure: a review of 86 cases (2004 to 2005) with implications for prognosis. *Am J Surg Pathol* 2013;**37**:890–7.
24. Kim SJ, Choisy SC, Barman P, Zhang H, Hancox JC, Jones SA *et al*. Atrial remodeling and the substrate for atrial fibrillation in rat hearts with elevated afterload. *Circ Arrhythm Electrophysiol* 2011;**4**:761–9.
25. Nowicki ER, Birkmeyer NJ, Weintraub RW, Leavitt BJ, Sanders JH, Dacey LJ *et al*. Multivariable prediction of in-hospital mortality associated with aortic and mitral valve surgery in Northern New England. *Ann Thorac Surg* 2004;**77**:1966–77.
26. Messika-Zeitoun D, Bellamy M, Avierinos JF, Breen J, Eusemann C, Rossi A *et al*. Left atrial remodelling in mitral regurgitation–methodologic approach, physiological determinants, and outcome implications: a prospective quantitative Doppler-echocardiographic and electron beam-computed tomographic study. *Eur Heart J* 2007;**28**:1773–81.
27. John B, Stiles MK, Kuklik P, Chandy ST, Young GD, Mackenzie L *et al*. Electrical remodelling of the left and right atria due to rheumatic mitral stenosis. *Eur Heart J* 2008;**29**:2234–43.
28. Nathan H, Eliakim M. The junction between the left atrium and the pulmonary veins. An anatomic study of human hearts. *Circulation* 1966;**34**:412–22.
29. Mouws E, Lanters EAH, Teuwen CP, van der Does L, Kik C, Knops P *et al*. Impact of ischemic and valvular heart disease on atrial excitation: a high-resolution epicardial mapping study. *J Am Heart Assoc* 2018;**7**:e008331.
30. Mouws E, Kik C, van der Does L, Lanters EAH, Teuwen CP, Knops P *et al*. Novel insights in the activation patterns at the pulmonary vein area. *Circ Arrhythm Electrophysiol* 2018;**11**:e006720.
31. Seemann G, Hoper C, Sachse FB, Dossel O, Holden AV, Zhang H. Heterogeneous three-dimensional anatomical and electrophysiological model of human atria. *Philos Trans A Math Phys Eng Sci* 2006;**364**:1465–81.
32. Aslanidi OV, Colman MA, Stott J, Dobrzynski H, Boyett MR, Holden AV *et al*. 3D virtual human atria: a computational platform for studying clinical atrial fibrillation. *Prog Biophys Mol Biol* 2011;**107**:156–68.
33. Krogh-Madsen T, Abbott GW, Christini DJ. Effects of electrical and structural remodeling on atrial fibrillation maintenance: a simulation study. *PLoS Comput Biol* 2012;**8**:e1002390.
34. Tobon C, Ruiz-Villa CA, Heidenreich E, Romero L, Hornero F, Saiz J. A three-dimensional human atrial model with fiber orientation. Electrograms and arrhythmic activation patterns relationship. *PLoS One* 2013;**8**:e50883.
35. Houben RP, de Groot NM, Smeets JL, Becker AE, Lindemans FW, Allessie MA. S-wave predominance of epicardial electrograms during atrial fibrillation in humans: indirect evidence for a role of the thin subepicardial layer. *Heart Rhythm* 2004;**1**:639–47.
36. van der Does L, Knops P, Teuwen CP, Serban C, Starreveld R, Lanters EAH *et al*. Unipolar atrial electrogram morphology from an epicardial and endocardial perspective. *Heart Rhythm* 2018;**15**:879–87.
37. Kumar S, Michaud GF. Unipolar electrogram morphology to assess lesion formation during catheter ablation of atrial fibrillation: successful translation into clinical practice. *Circ Arrhythm Electrophysiol* 2013;**6**:1050–2.
38. Roberts-Thomson KC, Stevenson I, Kistler PM, Haqqani HM, Spence SJ, Goldblatt JC *et al*. The role of chronic atrial stretch and atrial fibrillation on posterior left atrial wall conduction. *Heart Rhythm* 2009;**6**:1109–17.
39. Ho SY, Anderson RH, Sanchez-Quintana D. Gross structure of the atriums: more than an anatomic curiosity? *Pacing Clin Electrophysiol* 2002;**25**:342–50.
40. Becker AE. How structurally normal are human atria in patients with atrial fibrillation? *Heart Rhythm* 2004;**1**:627–31.